

# InFeR: Informed Failure Resilience in Learned Visual Navigation Control

Zishuo Wang<sup>1</sup> and Joel Loo<sup>1</sup> and David Hsu<sup>1</sup>

**Abstract**—While imitation learning (IL) has enabled successful visual navigation in many common environments, IL policies are prone to unpredictable failures under out-of-distribution (OOD) scenarios. This necessitates *failure-resilient* policies, which not only detect failures, but also recognise their sources and recover from them autonomously. We propose *InFeR*, a general framework for building IL policies with *informed failure resilience* without failure or recovery demonstrations. InFeR retrains an IL policy with a Variational Information Bottleneck (VIB) loss to structure its latent space for OOD failure detection. It applies a visual explainability technique, Grad-CAM, to localise an image region as the source of failure and inform a heuristic policy for recovery. All these are achieved without requiring additional training data. Real-world experiments show that InFeR enables informed failure recovery across two different policy architectures, yielding robust long-range navigation in complex environments.

## I. INTRODUCTION

Visual navigation is an attractive approach to robot navigation, leveraging rich visual information from low-cost sensors [1]. Imitation learning (IL) has emerged as a key method to learn visual navigation policies [2]–[4], but is inherently limited by training data. IL policies may fail unpredictably on inputs outside the training distribution, often without clear explanation [5]–[7]. We consider the problem of building IL policies with **informed failure resilience**, which we argue extends beyond detecting failures to also encompass autonomous, informed recovery from failures.

Current works addressing failure have two key limitations. First, they focus on detecting failures, with handling often limited to triggering operator interventions [8], [9]. Second, they often rely on external failure detectors, which lack access to policies’ internal representations and distributions and may fail to capture their true failure modes [10]. These limitations motivate three desiderata for failure-resilient policies: **(i)** the ability to autonomously *recover* from failures; **(ii)** the ability to *recognise* failure sources to inform recovery; and **(iii)** detection and recognition grounded in the policy’s internal representations to capture its true failure modes.

We propose **InFeR**, a general framework for building informed, failure-resilient visual navigation policies *without any failure or recovery demonstrations*. InFeR operates within the standard offline IL setting, learning policies from a single, static dataset of successful demonstrations, where failures are naturally approximated as scenarios outside the dataset’s distribution [6], [7], [11], [12]. InFeR introduces a

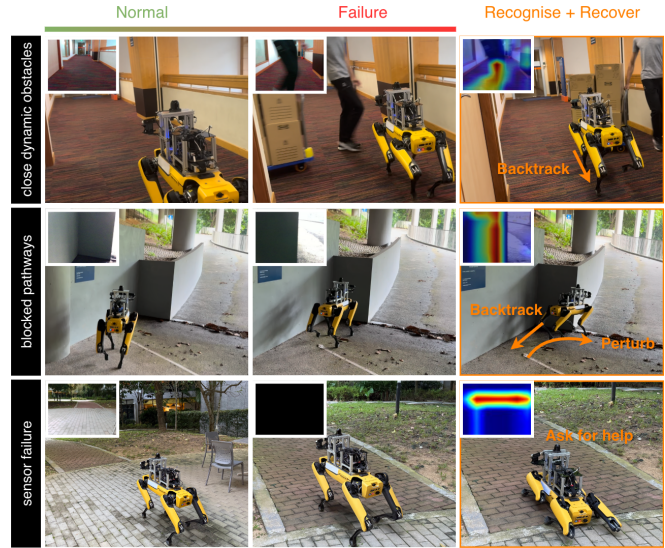


Fig. 1. **InFeR enables autonomous recovery from policy failures.** Limited training data causes failures in OOD scenarios (e.g. sensor failures, close dynamic obstacles etc.). InFeR *detects* these, and further *recognises* failure sources in the input image, enabling *informed failure recovery*.

regularised training objective to equip the policy to detect and recognise out-of-distribution (OOD) elements in its inputs without additional data or changes to its architecture. To recover from OOD scenarios, InFeR pairs the IL policy with a recovery policy guided by OOD recognition. Learning a recovery policy is ill-posed since failure and recovery examples are absent from data. Instead, InFeR designs a heuristic to greedily distance the robot from the identified failure source, then perturb it back to a nominal, in-distribution state.

Specifically, InFeR retrains an IL policy on the original data, into an OOD-aware policy that detects OOD image inputs and localises the image regions responsible. This is done with a Variational Information Bottleneck (VIB) loss, which structures the latent space between vision encoder and action decoder to distinguish in- and out-of-distribution inputs. This enables us to compute an OOD detection score, and to apply Grad-CAM explainability methods to recognise OOD regions [13], [14]. As shown in Figure 1, InFeR handles diverse failure modes by detecting and recognising OOD elements (e.g. dynamic obstacles, close-up obstructions, sensor failures), then performs recovery informed in real-time by feedback from OOD recognition. We show that InFeR enables two policies—DECISION [2] and GNM [3]—to detect and recover from critical failures in the real world, enabling a robot to complete a challenging 300m indoor/outdoor route without intervention.

<sup>1</sup>School of Computing & Smart Systems Institute, National University of Singapore. {zishuo.wang, joell, dyhsu}@comp.nus.edu.sg

## II. RELATED WORK

### A. Learned visual navigation

Navigating purely with high-dimensional image inputs is challenging for classical robotic systems [1]. Recent progress in visual navigation is enabled by learning perceptual modules [15]–[17] or even entire policies end-to-end [2]–[4]. Among these, end-to-end imitation learning (IL) has proven especially effective [2]–[4], enabling robust navigation in the wild [18], [19]. However, such policies remain opaque and offer no indication of impending failure [10]. We address this by defining *informed failure resilience* for end-to-end IL policies and proposing InFeR, a framework to augment IL policies into failure-resilient policies.

### B. Failure detection

Robust visual navigation in open-world settings hinges on the ability to detect failures [20]. Some recent approaches learn from explicit failure data: BADGR [21] heuristically labels failures in collected training data post hoc, while others learn from human interventions that precede failures [22]–[24]. Notably, [24] combines this with novelty detection to capture both user-defined failures and OOD events.

Since imitation learning (IL) datasets typically include only successful trajectories, unsupervised failure detection without explicit failure data becomes crucial when learning policies with IL. Failure detection is often framed as identifying OOD inputs that lie outside the IL dataset’s distribution [6]. This can be approached via epistemic uncertainty estimation [25] using ensembles or Bayesian neural networks [10], but such methods are often too computationally intensive for real-time navigation with limited compute [9].

Alternative methods seek greater efficiency, often at the cost of using detectors external to the policy which may not fully capture its failure modes and tend toward overly conservative detections [10]. Autoencoders [6], [7] and density estimators [26], [27] are common approaches, but may not accurately capture the data distribution as they are trained on observations and exclude action data, often producing overly conservative detections [10]. [28] apply Random Network Distillation to learn an external detector for the joint observation-action distribution. FAIL-Detect [9] compares a range of OOD scoring approaches, and combines them with conformal prediction for OOD detection with statistical guarantees. Finally, some methods leverage LLMs to identify and explain failures [29], [30], though these lack efficiency and insight into the policy’s specific failure modes.

InFeR focuses on efficiency and on capturing the policy’s true failure modes, achieved by embedding failure detection within the IL policy.

### C. Failure recovery

Robust navigation requires not only the ability to detect failures, but also to independently recover from them. Existing approaches largely terminate the episode on detection, and seek human intervention [8], [10], [31]. A small subset of works attempts to autonomously recover from failure by executing predefined actions open-loop—*e.g.* returning to a

default state [7] or executing a default behaviour [6]. Some systems layer increasingly aggressive preset actions [32] to improve recovery chances. [33] further requests interventions and learns from subsequent recovery demonstrations.

InFeR emphasises robustness through autonomous recovery and highlights the importance of OOD recognition in providing cues for informed, efficient recovery. To build failure-resilient policies, InFeR combines OOD-aware policies with unified OOD detection and recognition embedded inside, with a recovery policy guided by recognition results.

## III. PROBLEM FORMULATION

IL for visual navigation learns a policy  $\pi_{\text{IL}} : \mathcal{O} \rightarrow \mathcal{A}$  from a dataset  $\mathcal{D} = \{(o_1, a_1), \dots, (o_N, a_N)\}$ , where  $o_i \in \mathcal{O}$  are RGB or depth images, and  $a_i \in \mathcal{A}$  are actions typically given as target velocities. An OOD-aware policy is  $\pi_{\text{IL-OD}} : \mathcal{O} \rightarrow \mathcal{A} \times \mathcal{B} \times \mathcal{M}$ , mapping observation  $o_t$  to action  $a_t$ , binary OOD detection  $b_t \in \mathcal{B}$  and a representation of the location of OOD regions influencing the detection,  $M_t \in \mathcal{M}$ . We seek to obtain  $\pi_{\text{IL-OD}}$ , given a specific policy network architecture and  $\mathcal{D}$ . Since many IL datasets only contain successful demonstrations,  $\pi_{\text{IL-OD}}$  must be obtained without requiring additional failure data. We also seek to obtain  $\pi_{\text{Rec}}$ , a recovery policy which modulates or overrides  $\pi_{\text{IL-OD}}$  to take corrective actions in OOD scenarios, selecting appropriate actions on the basis of spatial feedback from OOD recognition  $M_t$ .  $\pi_{\text{Rec}}$ ’s actions either recover the robot to an in-distribution state, or halt it and call for external assistance if recovery is not possible.  $\pi_{\text{IL-OD}}$  and  $\pi_{\text{Rec}}$  together constitute a failure-resilient policy.

## IV. APPROACH

**InFeR** (Figure 2) provides a framework to modify visual navigation policies trained with IL,  $\pi_{\text{IL}}$ , into OOD-aware policies,  $\pi_{\text{IL-OD}}$ . It also provides a heuristic recovery policy,  $\pi_{\text{Rec}}$ , that makes corrective actions in OOD scenarios based on OOD recognition information from  $\pi_{\text{IL-OD}}$ .

### A. OOD-aware learned navigation policy, $\pi_{\text{IL-OD}}$

OOD-awareness involves detecting OOD scenarios and pinpointing the corresponding OOD regions in the visual input. We emphasise that OOD-awareness should be task-relevant, identifying OOD scenarios and pinpointing OOD regions related to failures on the navigation task the policy is trained for. Our policy,  $\pi_{\text{IL-OD}}$ , takes an image input  $I_t \in \mathbb{R}^{3 \times H \times W}$  and outputs action  $a_t$ , a binary OOD flag  $b_t$ , and a heatmap  $M_t \in \mathbb{R}^{H \times W}$  that identifies the OOD features in  $I_t$ . InFeR augments a policy  $\pi_{\text{IL}}$  into an OOD-aware one in two phases. First, during training, a structured latent space capturing task-relevant factors from  $I_t$  is learned by augmenting behaviour cloning with additional regularisation. Second, during inference, conformal prediction and Grad-CAM are applied to features from the policy’s latent space for OOD detection and recognition respectively.

**Learning task-relevant OOD-awareness with VIB.** We learn task-relevant latent representations  $Z$ , with the Variational Information Bottleneck [34]. This compresses input

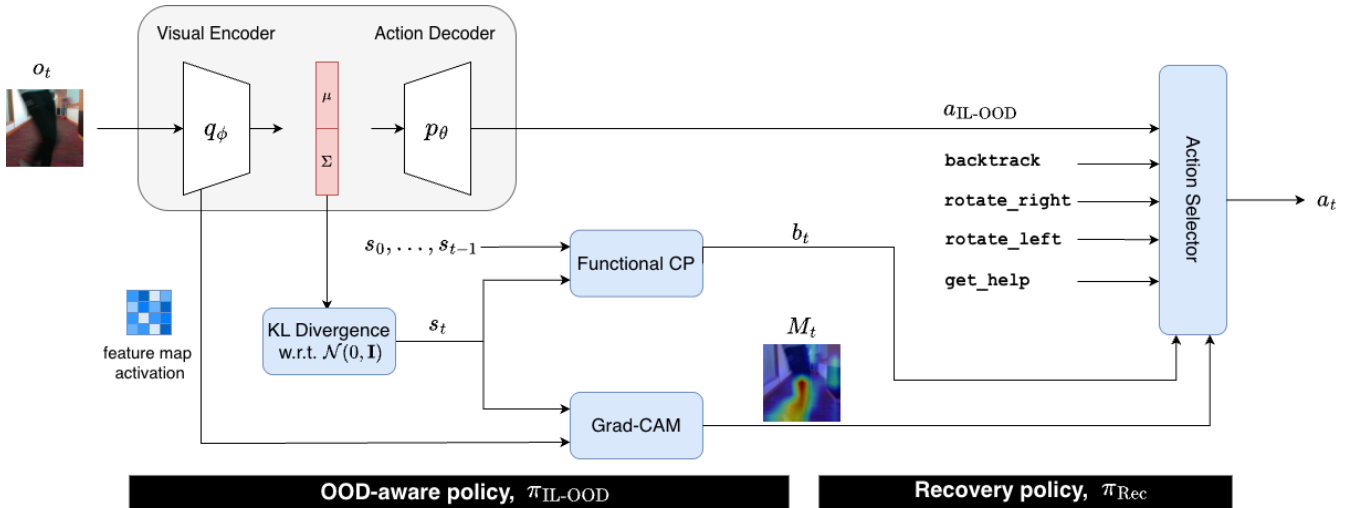


Fig. 2. **InFeR framework for informed failure resilience.** InFeR achieves informed failure resilience through augmenting learned policies with OOD-awareness. Apart from generating actions, OOD-aware policies also detect when OOD inputs are encountered ( $b_t$ ) and localise the OOD features in the observations ( $M_t$ ). Detection and recognition enable informed recovery from OOD or failure scenarios. InFeR employs a heuristic recovery policy taking  $b_t, M_t$  as inputs.

observations  $O$  into  $Z$ , while maximally retaining information crucial to predicting output actions  $A$ . Given  $I(\cdot; \cdot)$  as mutual information, we maximise:

$$\mathcal{L}_{\text{VIB}} = I(A; Z) - \beta I(Z; O) \quad (1)$$

Following [34], we apply variational approximations to optimise this intractable objective, yielding the loss:

$$\max_{\phi, \theta} \frac{1}{|\mathcal{D}|} \sum_{(o, a) \in \mathcal{D}} \mathbb{E}_{q_{\phi}(z|o)} [\log p_{\theta}(a|z)] - \beta \text{KL}[q_{\phi}(z|o) \| p(z)] \quad (2)$$

where  $q_{\phi}, p_{\theta}$  are the visual encoder and action decoder, respectively. The first term simplifies to a behaviour cloning loss, while the second term regularises the latent representation  $Z$  to stay close to prior  $p(z)$ , which we define as a unit Gaussian  $\mathcal{N}(0, \mathbf{I})$ . This regularisation means that at inference, an OOD input  $\hat{o}$  is likely to produce latent feature  $\hat{z}$  that diverges significantly from the prior. Thus the KL divergence  $\text{KL}[q_{\phi}(z|o) \| \mathcal{N}(0, \mathbf{I})]$  can serve as an effective scalar score indicative of OOD inputs during inference.

Learning with VIB can be viewed as augmenting a standard IL setup with additional regularisation of the latent features between a policy’s visual encoder and action decoder. This serves as a lightweight approach to instill task-relevant OOD-awareness into IL policies spanning a range of architectures, without supervision using explicit failure data.

**OOD detection with conformal prediction.** Binary detection  $b_t$  involves thresholding scalar OOD scores, but setting appropriate thresholds is challenging, especially since the threshold may be time-varying due to changing dynamics and scene appearance [9]. Conformal prediction (CP), particularly functional CP, offers a principled, distribution-free way to compute thresholds by generating a prediction band  $C_{\alpha}$  at a user-defined significance level  $\alpha \in [0, 1]$ . Under mild assumptions,  $C_{\alpha}$  contains the true score with probability

$1 - \alpha$ , enabling confident rejection of scores outside the band [9], [35]. Functional CP is an efficient, training-free method that wraps around a sequence of scores from any model.

We apply functional CP to a calibration set of trajectories to obtain time-varying thresholds on the KL scores. Similar to [9], we predict a one-sided  $C_{\alpha}$  that provides an upper bound on whether a score is in-distribution with probability  $1 - \alpha$ . We calibrate on a held-out split from the IL dataset,  $\mathcal{C}$ . We chunk trajectories into segments of  $T$  steps to standardise length, obtaining  $\mathcal{C}_{\text{scores}} = \{(s_{i,0}, \dots, s_{i,T}) : i = 1, \dots, |\mathcal{C}|\}$ . Following [35], we split  $\mathcal{C}$  into  $\mathcal{C}_{\mu}$  to compute the mean score across trajectories for each timestep, and  $\mathcal{C}_w$  to compute the width of the band  $C_{\alpha}$ . Given the mean scores  $\mu = (s_0, \dots, s_T)$ ,  $w$  is computed based on the maximum deviations from  $\mu$  per trajectory. Specifically, given

$$S = \{d_j : j = 1, \dots, |\mathcal{C}_w|\} \text{ where } d_j = \max_{t \in [0, T]} \{s_t - \mu_t\}, \quad (3)$$

$w$  is the  $(1 - \alpha)$ -quantile of  $S$ . The prediction band is the set of intervals  $\{[-\infty, \mu_t + w] : t = 1, \dots, T\}$ , where scores above the upper bound are rejected as OOD.

**OOD recognition with Grad-CAM.** Recognition aims to identify regions in observations  $o \in \mathcal{O}$  which contribute to the OOD detection. To do so, we apply Grad-CAM [13], a visual explanation method for interpreting CNN outputs. Grad-CAM is a training-free module integrated into  $\pi_{\text{IL-OOD}}$  at test time, offering efficiency as it requires only a single backward pass through the visual encoder.

Grad-CAM produces recognition heatmaps that highlight spatial regions influencing the model’s predictions. It computes gradients of the prediction with respect to feature map activations in preceding convolutional layers, obtaining weights capturing the contribution of each feature map to the prediction. To localise OOD-related visual features, we apply Grad-CAM on the KL-based OOD scores predicted by the

model. As deeper layers tend to capture higher-level semantic concepts (e.g. object parts) [36], we use Grad-CAM on the last layer of the visual encoder  $q_\phi$  to encourage meaningful recognition results. Specifically, we compute the weight for the  $k$ -th feature map of the layer as:

$$\alpha_k = \frac{1}{N} \sum_i \sum_j \frac{\partial \text{KL}[q_\phi(z_t|o_t) || \mathcal{N}(0, \mathbf{I})]}{\partial A_{ij}^k} \quad (4)$$

where  $A^k$  is the  $k$ -th feature map and  $N$  normalises across all  $A^k$ . The recognition result is:

$$M_{\text{Grad-CAM}} = \text{ReLU} \left( \sum_k \alpha_k A^k \right) \quad (5)$$

The resulting  $M_{\text{Grad-CAM}}$  has the same dimensions as  $A^k$ , which we upsample with bilinear interpolation to obtain  $M$ .

### B. Heuristic recovery policy, $\pi_{\text{Rec}}$

The recovery policy aims to take informed corrective actions when OOD scenarios are detected, and otherwise pass through  $\pi_{\text{IL-OOD}}$ 's actions during normal operation. Our policy,  $\pi_{\text{Rec}}$ , selects the appropriate corrective action from a discrete set of macro-actions. This set is designed to provide primitives that (i) *backtrack* the robot through known safe states, (ii) *perturb* it out of the OOD scenario, (iii) halt the robot and *seek human assistance*, if recovery is unrealistic and some termination condition is reached. We define the appropriate corrective action to be that which maximally avoids OOD features in the observation  $o_t$ .  $\pi_{\text{Rec}}$  uses the OOD recognition heatmap  $M_t$  to identify OOD features and inform selection of corrective actions.

Concretely,  $\pi_{\text{Rec}}$ 's action set comprises `{backtrack, rotate_left, rotate_right, get_help}`.  $\pi_{\text{Rec}}$  selects among the first 3 actions during recovery, with `get_help` triggered only after  $t_{\text{max\_tries}}$  attempts to recover without returning to a non-OOD state as indicated by  $b_t$ . To select among the first 3 actions, we discretise  $M_t$  along the horizontal axis into 3 bins. Each bin is marked as containing OOD features if the sum of pixel values exceeds a threshold.  $\pi_{\text{Rec}}$  selects `rotate_left/rotate_right` if the right/left bins are OOD, to perturb the robot away from the OOD region. Otherwise, it will `backtrack`, which executes a cached sequence of past actions in reverse.

## V. EXPERIMENTS

We evaluate three hypotheses: **(H1)** InFeR produces OOD-aware policies that are effective at task-relevant OOD detection and recognition. **(H2)** Our InFeR policy is effective at recovering from failures of the original visual navigation policy. **(H3)** InFeR is applicable across different visual navigation policies.

Section V-A validates **H1** by comparing against selected baselines on a collected test set, comprising RGB data from 3 Realsense D435i cameras collectively covering a 140° horizontal FoV. Section V-B validates **H2** and **H3** through real-world experiments on a Boston Dynamics Spot robot with the above Realsense setup, with the policies running onboard

TABLE I  
SELECTED BASELINES FOR OOD DETECTION/RECOGNITION.

Type	Method	Det.	Loc.	Inputs
<i>Density</i>	<i>NF</i> [26]	Density	-	$O_t$
<i>One-class</i>	<i>RND</i> [28]	Novelty	-	$O_t, A_t$
<i>Recon</i>	<i>AE</i> [6]	Recon	Recon	$O_t$
	<i>VAE-R</i>	Recon	Recon	$O_t$
	<i>VAE-KL</i>	KL	Grad-CAM	$O_t$
<i>InFeR (BC)</i>	<i>InFeR-INet</i>	KL	Grad-CAM	$O_t, A_t$
	<i>InFeR-DEC</i>	KL	Grad-CAM	$O_{t-H}, \dots, O_t, A_t$

an Nvidia Orin AGX. Finally, we demonstrate the potential of InFeR to improve navigation with learned controllers by showing that it enables effective failure recovery, allowing a learned controller to successfully complete a long-range route (Figure 6).

We train our policies and baselines on the training dataset from [2], comprising 30 hours of teleoperated trajectories demonstrating the task of path-following navigation in indoor and outdoor scenes. We identify four types of critical Navigation Failures (NF) to detect and recover from, which are OOD for this dataset:

- NF1 Sensor failure.** The robot receives blacked out images. The expected outcome is to seek human assistance, as the robot cannot recover on its own.
- NF2 Blocked pathways.** The robot's path is blocked by obstacles or untraversable regions. Since the dataset's trajectories focus on following clear paths, this is OOD. We consider (i) *local minima*, from which recovery is possible through a short sequence of local, reactive actions, and also (ii) *dead-ends*, which require substantially longer interventions or replanning to escape, and are irrecoverable for a local navigation policy.
- NF3 Close-range dynamic obstacles.** Sudden dynamic obstacles appearing close to the robot. As successful demonstrations avoid dynamic obstacles at a distance, such situations are OOD. The expected outcome is to halt and backtrack/perturb away from the sudden obstacle, then resume navigation along the path.
- NF4 Infeasible image goals.** Specific to image goal-conditioned policies where the goal is dissimilar to current observations. We focus on the irrecoverable case where the goal is not locally reachable, and the expected outcome is for the robot to seek human assistance.

### A. OOD detection and recognition

We evaluate performance of OOD-aware policies on OOD detection and recognition, comparing them against selected baselines (Table I). The OOD-aware policies are based on INet [18] and DECISION [2]. The baselines belong to three common classes: *density-based* approaches learn a density estimator for the training distribution; *one-class discriminators* learn to output a continuous metric without directly modelling the training distribution; *reconstruction-based* approaches indirectly model the training distribution

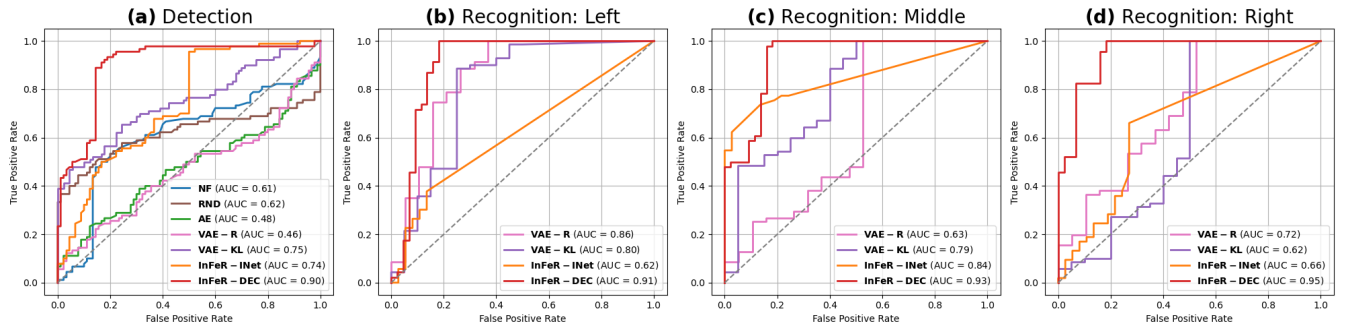


Fig. 3. **Comparison to baselines for OOD detection and recognition.** (a) ROC curves for OOD detection across CP significance levels  $\alpha$ . (b-d): ROC curves for OOD recognition, based on scores from summing pixels across the heatmap. We compute scores per heatmap bin: *Left, Middle, Right*.

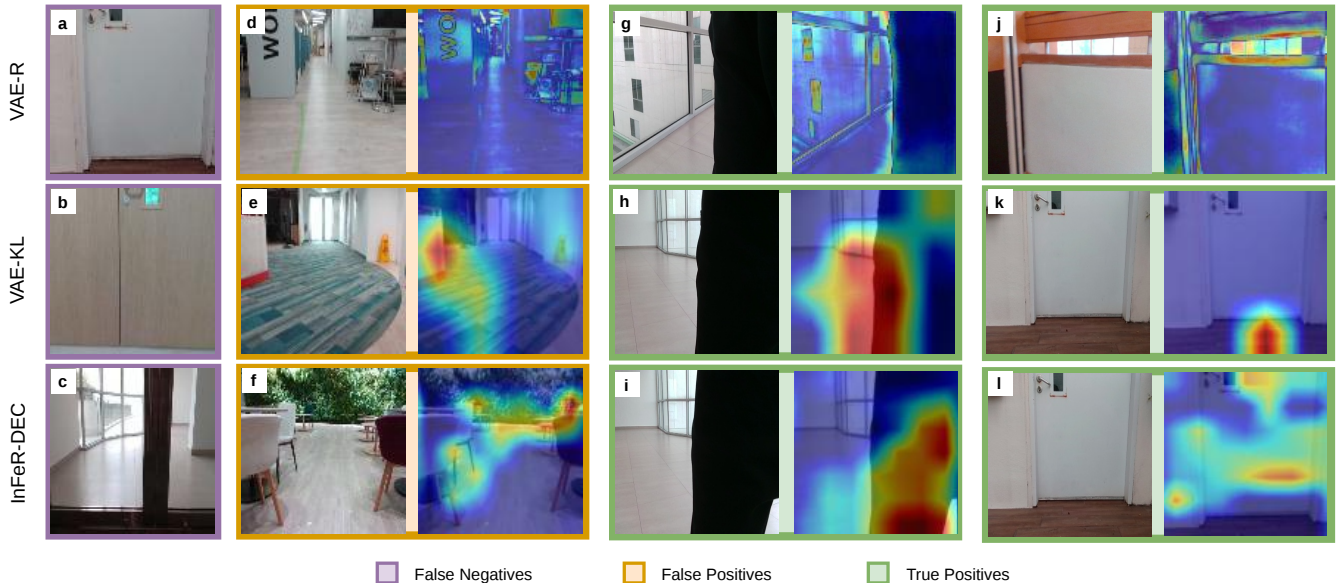


Fig. 4. **OOD detection and recognition examples.** We visualise selected reconstruction and InFeR methods. (a-c): Reconstruction-based methods struggle to detect failures like blocked pathways when there are few visual features. (d-f): VAE-R indiscriminately highlights high-frequency features, falsely detecting failures. InFeR-DEC is sensitive to obstacles (e.g. chairs, tables), prematurely triggering a detection. (g-l): VAE-KL offers smoother detections than VAE-R, but may not identify areas directly impacting navigation. In contrast, InFeR-DEC correctly highlights the agent’s leg (i) and the door (l) as failure causes.

by learning to reproduce observations, with post-hoc metrics applied to detect and recognise OOD inputs.

For density-based methods, we fit a normalising flow (NF) to observations with a Gaussian prior, using estimated likelihoods as the OOD score. For one-class discriminators, we use Random Network Distillation (RND) [28], which trains a predictor to map training data to output of a fixed random function, using prediction error as a measure of sample novelty and the OOD score. In prior art, these two approaches detect OOD inputs but do not support recognition. Reconstruction-based methods include autoencoders (AE) [6] and variational autoencoders (VAE-R) [7]. We apply post-hoc metrics based on reconstruction error: mean-squared error for OOD detection, and pixel-wise errors for recognition. Since InFeR’s detection/recognition metrics apply to any VIB-based model, we test them with VAE-KL, which shares weights with VAE-R, but uses KL scores and Grad-CAM for OOD detection and recognition instead.

We collect a test set of 180 trajectories: 90 with a single

failure near the end, and 90 normal (Figure 1). Failures are evenly distributed across three types—sensor failure, blocked paths, and close-range dynamic obstacles (NF1-NF3). We exclude infeasible image goals, which is a failure specific to image goal-conditioned architectures. Half the trajectories are in novel office and garden environments; the rest are in novel areas that resemble training data. Each trajectory is 10s long, with failures occurring at the 8s mark. A failure is detected if any frame from 8s onward is classified as OOD. To annotate ground-truth recognition, we divide each frame vertically into three bins and mark the bins containing features related to navigation failure (e.g. dynamic objects, blockages), similar to the approach in Section IV-B.

We illustrate OOD detection performance via ROC curves across CP significance levels  $\alpha$ . To evaluate recognition independently of detection, we restrict analysis to failure trajectories and, for each method, to the detections obtained at a true positive rate of 0.9, normalising detection sensitivity across methods. On this subset, we compute per-bin ROC

TABLE II

EVALUATION OF INFER POLICIES. INFER IS APPLIED TO GNM [3] AND DECISION [2]. A “BLIND” VARIANT THAT DOES NOT USE RECOGNITION RESULTS, AND RANDOMLY SELECTS CORRECTIVE ACTIONS ON OOD DETECTIONS IS ALSO EVALUATED.

Failure type	Recoverable	InFeR-GNM			InFeR-DEC			InFeR-DEC-Blind		
		Det. SR	Han. SR	Time (s)	Det. SR	Han. SR	Time (s)	Det. SR	Han. SR	Time (s)
Sensor failure	✗	1	1	10.00	1	1	5.00	1	1	5.00
Blocked (Dead-end)	✗	-	-	-	1	1	8.48	1	0.7	17.39
Blocked (Local minima)	✓	-	-	-	1	0.8	6.66	1	0.7	10.39
Close-range dynamic obs.	✓	0.9	0.7	8.21	0.9	0.8	1.97	0.9	0.5	1.95
Infeasible image goal	✗	1	1	16.00	-	-	-	-	-	-

curves for the recognition heatmap, with scores given by  $\mathbb{I}[b_t = 1] \sum_{m \in M_{t,k}} m$ , where  $b_t = 1$  is an OOD detection, and  $M_{t,k}$  is the  $k$ -th bin of the heatmap  $M_t$ . This yields the per-bin recognition score only when the input is flagged as OOD. The results in Figure 3 support **H1**: InFeR produces OOD-aware policies effective at task-relevant OOD detection/recognition. We draw three conclusions:

**OOD-aware policies outperform existing methods.** InFeR’s approach of integrating OOD detectors into IL policies outperforms state-of-the-art OOD detection and recognition approaches, supporting **H1**. Both InFeR methods achieve high AUC scores across *both* detection and recognition compared with density-based approaches (NF), one-class discriminators (RND), and reconstruction-based approaches (AE, VAE-R). InFeR-DEC achieves the best performance by a clear margin, with high TPR and relatively few false positives. It also outperforms InFeR-INet, since its temporally accumulated features offer richer information to distinguish OOD scenarios. Unlike other methods that detect and recognise independently of the policy (*e.g.* VAE-R, VAE-KL), InFeR embeds both in the policy, reducing computation.

**KL scores, Grad-CAM are most effective metrics.** Results for *Recon* and *InFeR* methods indicate that approaches using KL-based OOD scores for detection and Grad-CAM for recognition perform best at their respective tasks. AE and VAE-R show similar poor performance on detection and recognition when using MSE and pixel-wise reconstruction error respectively. However, VAE-KL achieves significantly stronger performance on both tasks despite having the same model weights as VAE-R, differing only in the use of KL scores and Grad-CAM as OOD measures. We attribute this to the fact that KL scores and Grad-CAM operate on *latent vectors* instead of high-dimensional reconstructed images. As latent vectors are compressed representations that learn to focus on task-relevant factors, they are less noisy information sources than reconstructed images. Qualitative analysis (Figure 4) bears this out: recognition results from VAE-R are significantly noisier than VAE-KL or InFeR methods, and overfit to high-frequency artifacts in the inputs. While recent works shift the focus to methods like density-based [26] or second-order [9], [37] approaches, we highlight that selecting the right OOD measures enables reconstruction methods to outperform these. This also validates InFeR’s choice of scores for OOD detection and recognition.

**Action supervision improves OOD recognition.** We hypothesised that learning from both observations and actions

encourages more task-relevant representations. Observation-only methods (*e.g. Recon*) perform comparably on detection. However, adding actions enables better, task-relevant OOD recognition: in Figure 4(*k, l*), InFeR-DEC highlights features relevant to the path-following task (a closed door), whereas VAE-KL highlights irrelevant textures on the floor.

### B. Failure resilient navigation in the real world

We evaluate InFeR’s effectiveness in enabling failure-resilient navigation in the real world, across different policy architectures. Specifically, we test whether InFeR policies can detect and recover from the key failure types identified (**NF1–NF4**). To illustrate the importance of informed failure resilience, we show that InFeR allows the DECISION policy to autonomously complete a 300m route with varied terrain (cluttered indoor plaza, outdoor park with forested paths) despite critical failures.

We test two policies with differing architectures: InFeR-GNM, based on the General Navigation Model [3], an image goal-conditioned policy combining CNN encoders with MLP heads; InFeR-DEC, based on DECISION, a policy that contains recurrent elements and has a more complex structure to explicitly handle multimodality in navigation tasks. InFeR-GNM is evaluated on all failure types except blocked pathways (**NF2**), since occlusion of the goal in dead-ends or local minima makes this failure mode similar to that of infeasible goals (**NF4**). Conversely, since InFeR-DEC learns path-following skills and has no goal conditioning, it is tested on all failure types except infeasible goals. For each failure type, we run 10 trials, triggering a failure after  $\sim 8$ s of normal operation. We report detection success rate (Det. SR), combined detection and recovery success rate (Han. SR), and time taken from first detection to recovery. Overall, we draw three specific conclusions:

**InFeR effectively recovers from diverse real-world failures.** Table II shows that InFeR enables high detection and recovery success across varied failure types, supporting **H2**. It performs especially well in irrecoverable scenarios, where consistent, robust OOD detection while the robot perturbs is needed to appropriately terminate recovery efforts and request human help. While overall detection is stable, InFeR-DEC occasionally fails in local minima due to spurious heatmap activations that guide the robot back into the minima. The exploration strategy can be improved to mitigate this by adding memory or temporally filtering the heatmap. InFeR also responds effectively to close-range dynamic ob-

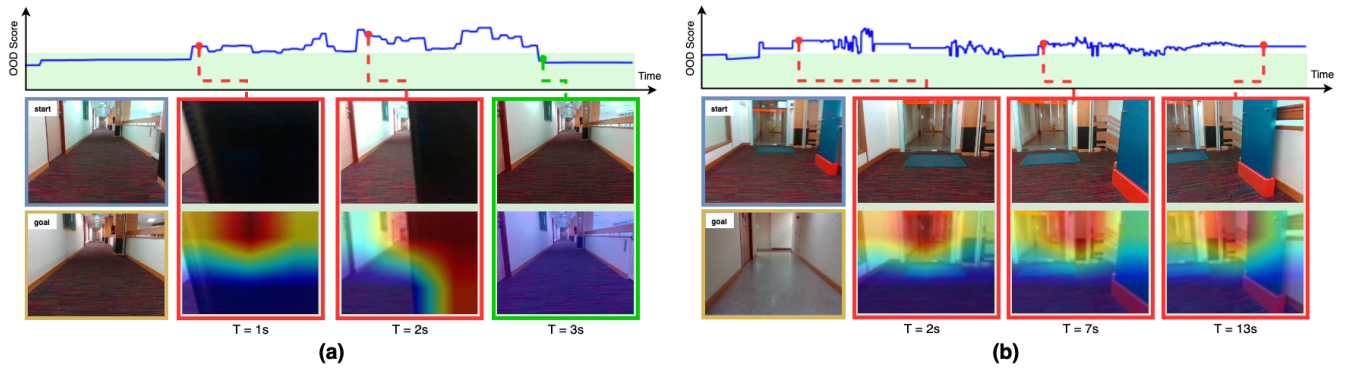


Fig. 5. **Informed failure recovery with InFeR-GNM.** (a): Robot is blocked by a pedestrian passing close by in front. It first backtracks ( $T=1s$ ) to avoid the pedestrian, recognises the pedestrian on its right ( $T=2s$ ) and pivots in the opposite direction to recover ( $T=3s$ ). (b): Robot is issued an infeasible goal behind the glass door. It perturbs locally to various directions, but finds itself always blocked by obstacles, thus terminating and seeking help.

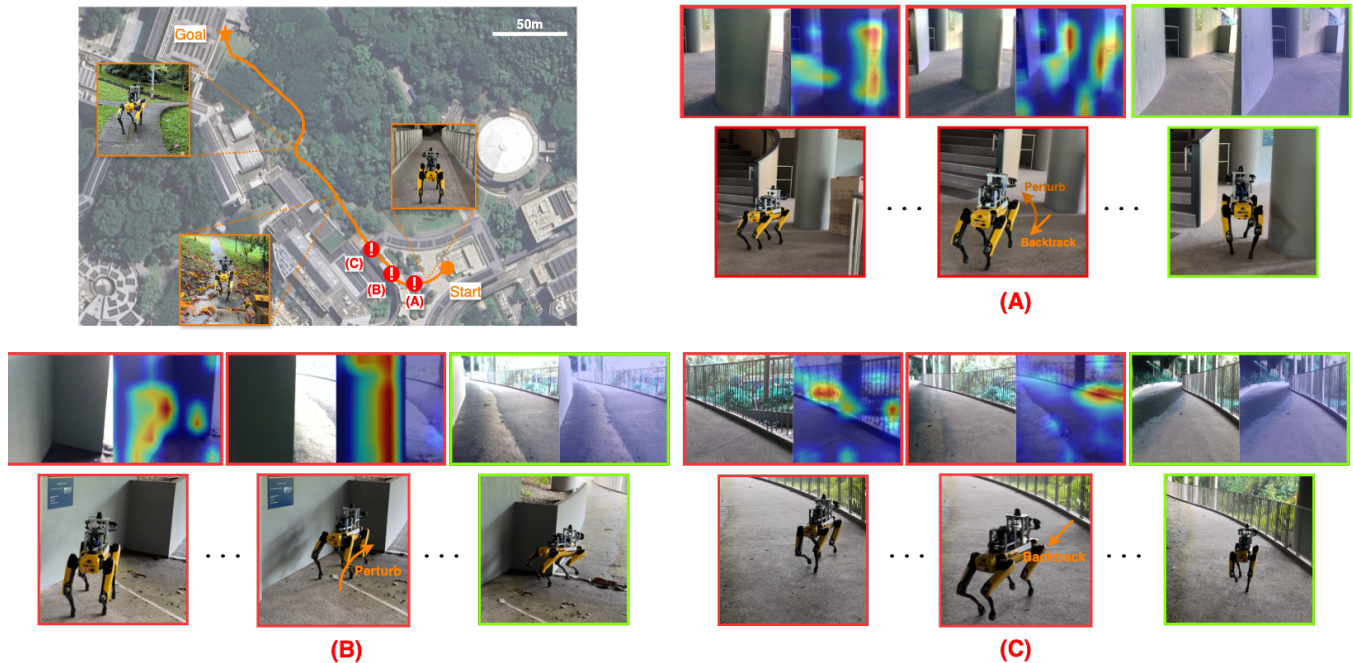


Fig. 6. **Informed recovery enables long-range navigation with InFeR-DEC.** The robot navigates a 300m route starting indoors then crossing a park. It recovers from the three failures shown: (A): stuck in local minima due to clutter, has to backtrack and perturb to find a path; (B): stuck in a corner, has to perturb to the right to continue on the path; (C) heading towards a railing, unseen during training, has to backtrack and align itself along the path.

stacles, selecting timely corrective actions. Though InFeR-GNM shows slower recovery times due to gradual KL score decay, it still quickly responds with suitable behaviours like backtracking or perturbing away from obstacles (Figure 5).

**InFeR works across policy architectures.** Table II highlights InFeR’s consistent and strong performance across two policies (GNM and DECISION) despite their differing architectures and failure modes, supporting **H3**. InFeR-GNM’s effectiveness on infeasible image goals (**NF4**) shows that the VIB mechanism captures architecture-specific issues. Both InFeR-GNM and InFeR-DEC recover from common failures similarly well, underscoring InFeR’s generalisability. A key factor influencing performance is the resolution of the visual encoder’s final feature map. InFeR-DEC (Figure 6) has higher-resolution feature maps than the GNM (Figure 5), enabling finer recognition. This contributes to

the GNM’s poorer performance with close-range dynamic obstacles (**NF3**).

**OOD recognition is key to efficient, effective recovery.** We compare InFeR-DEC with an uninformed variant (InFeR-DEC-Blind) that ignores the recognition heatmap  $M_t$ , and randomly selects corrective actions. InFeR-DEC consistently outperforms InFeR-DEC-Blind, especially in recovering from close-range dynamic obstacles (**NF3**), where timely, informed actions are critical. While InFeR-DEC-Blind can occasionally recover in static environments via random perturbation, dynamic scenarios demand precise recognition. Thus, InFeR-DEC succeeds in 8/9 detected cases vs. 5/9 for InFeR-DEC-Blind. Informed recovery proves more efficient across all failure types, with InFeR-DEC recovering up to 2x faster than InFeR-DEC-Blind.

## VI. CONCLUSION

We argue that **informed failure resilience** in IL policies extends beyond detection to encompass recognising failure sources and autonomously recovering from them. This paper introduces **InFeR**, a general framework for building failure-resilient visual navigation policies *without failure or recovery demonstrations*. InFeR enables OOD detection and recognition grounded in the policy’s latent space, and pairs the policy with a separate recovery policy informed by real-time OOD recognition results. It requires no additional data, and no changes to the IL policy’s architecture. InFeR generalises across two distinct policy architectures, and a range of diverse failure modes across different scenes, enabling IL policies to succeed at long-range navigation in complex environments without intervention. This shows that InFeR is a clear step toward safe, robust navigation with IL. We will extend InFeR to policies with more advanced visual encoders [14], and to use more sophisticated recovery strategies.

## REFERENCES

- [1] F. Bonin-Font, A. Ortiz, and G. Oliver, “Visual navigation for mobile robots: A survey,” *Journal of Intelligent and Robotic Systems*, vol. 53, pp. 263–296, 2008.
- [2] B. Ai, W. Gao, D. Hsu *et al.*, “Deep visual navigation under partial observability,” in *International Conference on Robotics and Automation (ICRA)*, 2022.
- [3] D. Shah, A. Sridhar, A. Bhorkar, N. Hirose, and S. Levine, “Gnm: A general navigation model to drive any robot,” in *International Conference on Robotics and Automation (ICRA)*, 2023.
- [4] A. Sridhar, D. Shah, C. Glossop, and S. Levine, “Nomad: Goal masked diffusion policies for navigation and exploration,” in *International Conference on Robotics and Automation (ICRA)*, 2024.
- [5] R. Chalapathy and S. Chawla, “Deep learning for anomaly detection: A survey,” *arXiv preprint arXiv:1901.03407*, 2019.
- [6] C. Richter and N. Roy, “Safe visual navigation via deep learning and novelty detection,” in *Robotics: Science and Systems (RSS)*, 2017.
- [7] J. Wong, A. Tung, A. Kurenkov, A. Mandlekar, L. Fei-Fei, S. Savarese, and R. Martín-Martín, “Error-aware imitation learning from teleoperation data for mobile manipulation,” in *Conference on Robot Learning (CoRL)*, 2022.
- [8] C. Gokmen, D. Ho, and M. Khansari, “Asking for help: Failure prediction in behavioral cloning through value approximation,” in *International Conference on Robotics and Automation (ICRA)*, 2023.
- [9] C. Xu, T. K. Nguyen, E. Dixon, C. Rodriguez, P. Miller, R. Lee, P. Shah, R. Ambrus, H. Nishimura, and M. Itkina, “Can we detect failures without failure data? uncertainty-aware runtime failure detection for imitation learning policies,” *arXiv preprint arXiv:2503.08558*, 2025.
- [10] R. McAllister, G. Kahn, J. Clune, and S. Levine, “Robustness to out-of-distribution inputs via task-aware generative uncertainty,” in *International Conference on Robotics and Automation (ICRA)*, 2019.
- [11] C. Agia, R. Sinha, J. Yang, Z. Cao, R. Antonova, M. Pavone, and J. Bohg, “Unpacking failure modes of generative policies: Runtime monitoring of consistency and progress,” in *CoRL Workshop on Safe and Robust Robot Learning for Operation in the Real World*, 2024.
- [12] O. Çatal, S. Leroux, C. De Boom, T. Verbelen, and B. Dhoedt, “Anomaly detection for autonomous guided vehicles using bayesian surprise,” in *International Conference on Intelligent Robots and Systems (IROS)*, 2020.
- [13] R. R. Selvaraju, M. Cogswell, A. Das, R. Vedantam, D. Parikh, and D. Batra, “Grad-cam: Visual explanations from deep networks via gradient-based localization,” *International Journal of Computer Vision*, vol. 128, no. 2, p. 336–359, 2019.
- [14] S. Leem and H. Seo, “Attention guided cam: visual explanations of vision transformer guided by self-attention,” in *AAAI conference on artificial intelligence (AAAI)*, 2024.
- [15] J. Frey, M. Mattamala, N. Chebrolu, C. Cadena, M. Fallon, and M. Hutter, “Fast traversability estimation for wild visual navigation,” in *Robotics: Science and Systems (RSS)*, 2023.
- [16] X. Meng, N. Hatch, A. Lambert, A. Li, N. Wagener, M. Schmittle, J. Lee, W. Yuan, Z. Chen, S. Deng, G. Okopal, D. Fox, B. Boots, and A. Shaban, “Terrainet: Visual modeling of complex terrain for high-speed, off-road navigation,” in *Robotics: Science and Systems (RSS)*, 2023.
- [17] Z. Fang, A. Xiao, D. Hsu, and G. H. Lee, “From obstacles to etiquette: Robot social navigation with vlm-informed path selection,” *IEEE Robotics and Automation Letters*, vol. 11, no. 4, pp. 3947–3954, 2026.
- [18] W. Gao, B. Ai, J. Loo, and D. Hsu, “Intentionnet: Map-lite visual navigation at the kilometre scale,” *arXiv preprint arXiv:2407.03122*, 2024.
- [19] D. Shah and S. Levine, “ViKiNG: Vision-Based Kilometer-Scale Navigation with Geographic Hints,” in *Robotics: Science and Systems (RSS)*, 2022.
- [20] Q. Rahman, P. Corke, and F. Dayoub, “Run-time monitoring of machine learning for robotic perception: A survey of emerging trends,” *IEEE Access*, vol. 9, pp. 20 067–20 075, 2021.
- [21] G. Kahn, A. Villaflor, V. Pong, P. Abbeel, and S. Levine, “Uncertainty-aware reinforcement learning for collision avoidance,” *arXiv preprint arXiv:1702.01182*, 2017.
- [22] J. Spencer, S. Choudhury, M. Barnes, M. Schmittle, M. Chiang, P. Ramadge, and S. Srinivasa, “Learning from interventions: Human-robot interaction as both explicit and implicit feedback,” in *Robotics: Science and Systems (RSS)*, 2020.
- [23] H. Liu, S. Dass, R. Martín-Martín, and Y. Zhu, “Model-based runtime monitoring with interactive imitation learning,” in *International Conference on Robotics and Automation (ICRA)*, 2024.
- [24] H. Liu, Y. Zhang, V. Betala, E. Zhang, J. Liu, C. Ding, and Y. Zhu, “Multi-task interactive robot fleet learning with visual world models,” in *Conference on Robot Learning (CoRL)*, 2024.
- [25] M. Itkina and M. Kochenderfer, “Interpretable self-aware neural networks for robust trajectory prediction,” in *Conference on Robot Learning (CoRL)*, 2022.
- [26] L. Wellhausen, R. Ranfil, and M. Hutter, “Safe robot navigation via multi-modal anomaly detection,” *IEEE Robotics and Automation Letters*, vol. 5, no. 2, pp. 1326–1333, 2020.
- [27] X. Cai, S. Ancha, L. Sharma, P. R. Osteen, B. Bucher, S. Phillips, J. Wang, M. Everett, N. Roy, and J. P. How, “EVORA: Deep Evidential Traversability Learning for Risk-Aware Off-Road Autonomy,” *IEEE Transactions on Robotics*, vol. 40, pp. 3756–3777, 2024.
- [28] N. He, S. Li, Z. Li, Y. Liu, and Y. He, “ReDiffuser: Reliable decision-making using a diffuser with confidence estimation,” in *International Conference on Machine Learning (ICML)*, 2024.
- [29] R. Sinha, A. Elhafs, C. Agia, M. Foutter, E. Schmerling, and M. Pavone, “Real-time anomaly detection and reactive planning with large language models,” in *Robotics: Science and Systems (RSS)*, 2024.
- [30] E. Jin, Q. Feng, Y. Mou, G. Lakemeyer, S. Decker, O. Simons, and J. Stegmaier, “Logicad: Explainable anomaly detection via vlm-based text feature extraction,” in *AAAI Conference on Artificial Intelligence (AAAI)*, 2025.
- [31] S. Hecker, D. Dai, and L. Van Gool, “Failure prediction for autonomous driving,” in *Intelligent Vehicles Symposium (IV)*, 2018.
- [32] S. Macenski, F. Martín, R. White, and J. Ginés Clavero, “The marathon 2: A navigation system,” in *International Conference on Intelligent Robots and Systems (IROS)*, 2020.
- [33] F. Del Duchetto, A. Kucukyilmaz, L. Iocchi, and M. Hanheide, “Do not make the same mistakes again and again: Learning local recovery policies for navigation from human demonstrations,” *IEEE Robotics and Automation Letters*, vol. 3, no. 4, pp. 4084–4091, 2018.
- [34] A. A. Alemi, I. Fischer, J. V. Dillon, and K. Murphy, “Deep variational information bottleneck,” in *International Conference on Learning Representations (ICLR)*, 2017.
- [35] J. Diquigiovanni, M. Fontana, and S. Vantini, “The importance of being a band: Finite-sample exact distribution-free prediction sets for functional data,” *Statistica Sinica*, 2025.
- [36] A. Mahendran and A. Vedaldi, “Visualizing deep convolutional neural networks using natural pre-images,” *International Journal of Computer Vision*, vol. 120, no. 3, p. 233–255, 2016.
- [37] S. Ancha, P. R. Osteen, and N. Roy, “Deep evidential uncertainty estimation for semantic segmentation under out-of-distribution obstacles,” in *International Conference on Robotics and Automation (ICRA)*, 2024.